

1 **Using Eddy Covariance Observations to Determine the Carbon**  
2 **Sequestration Characteristics of Subalpine Forests in the Qinghai-**  
3 **Tibet Plateau**

4 Niu Zhu<sup>1,2,4</sup>, Jinniu Wang<sup>1,2</sup>, Dongliang Luo<sup>3</sup>, Xufeng Wang<sup>3</sup>, Cheng Shen<sup>1,2</sup>, Ning Wu<sup>1</sup>  
5 1 Chengdu Institute of Biology, Chinese Academy of Sciences, Chengdu 610041,  
6 China

7 2 Mangkang Ecological Monitoring Station, Tibet Ecological Security Barrier  
8 Ecological Monitoring Network, Qamdo 854500, China

9 3 Northwest Institute of Eco-environmental Resources, Chinese Academy of  
10 Sciences, Lanzhou 730000, China

11 4 College of Resources and Environmental Sciences, Gansu Agricultural University,  
12 Lanzhou 730070, China

13 **Correspondence:** Jinniu Wang (wangjn@cib.ac.cn)

14 **Abstract:** The subalpine forests are a crucial component of the carbon cycling system in the  
15 Qinghai-Tibet Plateau (QTP). However, there are significant data gaps in the QTP currently, it also  
16 essential to enhance continuous monitoring of forest carbon absorption processes in the future. This  
17 study investigates two years' carbon exchange dynamics of a subalpine forest on the QTP using the  
18 eddy covariance method. We first characterized its seasonal carbon dynamics of the subalpine forest,  
19 revealing the higher carbon dioxide exchange rates in summer and autumn and lower rates in winter  
20 and spring, and found that autumn is the peak period for carbon sequestration in the subalpine forest,  
21 with the maximum measured value of CO<sub>2</sub> absorption reaching 10.70 μmol m<sup>-2</sup> s<sup>-1</sup>. Subsequently,  
22 we examined the environmental factors influencing carbon sequestration function. The PCA  
23 analysis show that photosynthetically active radiation (PAR) was major environmental factor  
24 driving the net ecosystem CO<sub>2</sub> exchange (NEE), significantly influencing forest and carbon  
25 absorption, and the increase of relative humidity decreases the rate of carbon fixation. In addition,  
26 we explored NEE and its influencing factors at the regional scale, found that air temperature  
27 promotes carbon dioxide absorption (negative NEE values), while the average annual precipitation  
28 shows a minor effect on NEE. At the annual scale, the subalpine forest functions as a strong carbon  
29 sink, with an average NEE of -332~-351 g C m<sup>-2</sup> (from November 2020 to October 2022). Despite  
30 facing the challenges of climate change, forests remain robust carbon sinks with the highest carbon  
31 sequestration capacity in the QTP, with an average annual CO<sub>2</sub> absorption rate of 368 g C m<sup>-2</sup>. This  
32 study provides valuable insights into the carbon cycling mechanism in subalpine ecosystems and  
33 the global carbon balance.

34 **Keywords:** Subalpine forest; Qinghai-Tibet Plateau; The eddy covariance method; Three Parallel  
35 Rivers Region; Carbon sinks

## 36 1 Introduction

37 Carbon dioxide (CO<sub>2</sub>) is a prominent greenhouse gas, and its atmospheric concentration has  
38 reached an unprecedented high level in recent years, in May 2021, a recorded peak of 419 parts per  
39 million (ppm) was observed at the Mauna Loa Observatory in Hawaii (Stein, 2021). The global  
40 atmospheric CO<sub>2</sub> concentration is rapidly increasing at a rate of 2 to 3 ppm per year, compared to  
41 pre-industrial levels, the average global temperature has already risen by 1.1 °C by 2019 (World  
42 Meteorological Organization, 2019). Human activities have been the primary catalyst behind the

43 significant surge in atmospheric CO<sub>2</sub> concentrations (Schweizer et al., 2020). CO<sub>2</sub> and CH<sub>4</sub>  
44 collectively contribute approximately 70% to the global warming potential among the six  
45 greenhouse gases specified in the Kyoto Protocol (Zhang et al., 2022). As atmospheric CO<sub>2</sub>  
46 concentrations continue to rise, global climate warming is gradually intensifying. Therefore, The  
47 Paris Agreement urges national governments to restrict the increase in global average temperature  
48 to well below 2.0 °C above pre-industrial levels and to strive to limit it to 1.5 °C. The increasing  
49 atmospheric CO<sub>2</sub> levels will lead to irreversible ecological disasters. For instance, the concentration  
50 of CO<sub>2</sub> in the atmosphere is projected to double within approximately 50 years if global  
51 consumption of fossil fuels continues to rise at the current rate. Addressing the greenhouse effect  
52 caused by carbon dioxide and reducing its impact is a crucial challenge facing human society today.  
53 Reducing regional carbon emissions or per capita carbon emissions is widely regarded as an  
54 effective approach to carbon reduction (Wang et al., 2023a). Nevertheless, countries around the  
55 world have already begun to commit to carbon reduction and carbon neutrality efforts. On  
56 September 22, 2020, during the 75th session of the United Nations General Assembly, the Chinese  
57 government announced "double carbon" goals, which aim to achieve carbon emission peaking by  
58 2030 and carbon neutrality by 2060, in alignment with ecological conservation and sustainable  
59 development objectives (Yu, 2022). It is predicted that China's average forest carbon sequestration  
60 rate will reach 0.358 Pg C year<sup>-1</sup> by 2060 (Cai et al., 2022). This significant rate of carbon  
61 sequestration is expected to have a substantial impact on the environment and economy, providing  
62 negative feedback to global warming (Pan et al., 2011).

63 Currently, there are various methods available to accurately quantify the carbon sequestration  
64 potential of forests. Quantitative estimation of carbon sequestration potential still requires scientists  
65 to establish more *in-situ* sites and generate comprehensive datasets to assess a wide range of areas.  
66 Initially, individuals' biomass measurements were used to estimate forest carbon sequestration  
67 capacity (Ebermayer, 1876). However, this method was time-consuming, labor-intensive, and prone  
68 to inaccuracies due to the omission of various variables during the calculation process. The  
69 development of modeling techniques allowed for the use of simulation methods-forest management  
70 models and land ecosystem-climate interaction models, such as the Ecological Assimilation of Land  
71 and Climate Observation (EALCO), have been widely applied in this regard (Landsberg and Waring,

72 1997; Wang et al., 2001). Currently, remote sensing monitoring and the eddy covariance (EC)  
73 method are quite popular. Remote sensing techniques can be used to extract vegetation parameters  
74 (e.g., normalized difference vegetation index (NDVI)) from multispectral bands and estimate the  
75 carbon sequestration of entire forests through regression analysis (Laurin et al., 2014). The eddy  
76 covariance method, allowing continuous, long-term carbon flux calculation, provides fundamental  
77 data for model establishment and calibration. It has been widely applied across ecosystems,  
78 including urban areas, farmlands, grasslands, forests, and water bodies (Konopka et al., 2021; Vote  
79 et al., 2015; Du et al., 2022a; Kondo et al., 2017; Li et al., 2022).

80 The forest ecosystem's Net ecosystem exchange (NEE) of carbon dioxide is influenced by  
81 multiple environmental factors. Previous studies have shown that NEE is significantly influenced  
82 by air temperature (AT), photosynthetically active radiation (PAR), vapor pressure deficit (VPD),  
83 relative humidity (RH), and soil temperature (ST) (Liu et al., 2022). For instance, temperature  
84 variables, especially annual or seasonal average temperature variations, serve as the optimal single  
85 predictor for carbon flux, explaining variations in carbon flux between 19% and 71% (Banbury  
86 Morgan et al., 2021). PAR not only influences the absorption of carbon dioxide by the forest canopy  
87 but also affects the utilization of carbohydrates by roots due to its association with canopy processes  
88 and soil respiration (Baumgartner et al., 2020). Furthermore, research suggests that NEE is  
89 influenced by biotic factors such as NDVI and leaf area index (LAI) (Tang et al., 2022). Given the  
90 projected future global warming trends, forests play a highly significant vast carbon reservoir for  
91 their becoming worthy of attention. The Qinghai-Tibet Plateau (QTP) is the highest and largest  
92 plateau in the world, with an extensive area of alpine forests covering approximately  $2.3 \times 10^5$  km<sup>2</sup>,  
93 holding tremendous economic and ecological benefits. The southeastern region of the QTP boasts  
94 one of the world's highest-altitude subalpine forest ecosystems. Research indicates that the  
95 subalpine forest ecosystem in this area has a remarkable capacity to consume methane, reaching up  
96 to 5.06 kg ha<sup>-1</sup> yr<sup>-1</sup>, and playing a significant role in mitigating the impact of greenhouse gases (Qu  
97 et al., 2023). Since the 1960s, the QTP has experienced a faster warming rate than lowland areas, a  
98 phenomenon projected to intensify by the end of the 21st century (Li et al., 2019). Currently, the  
99 QTP is considered a weak carbon sink at the overall level, but the carbon source-sink dynamics vary  
100 among different ecosystems (Chen et al., 2022). For instance, most lakes in the QTP are currently

101 characterized by supersaturated CO<sub>2</sub> levels (Cole et al., 1994). Mu et al. (2023) found that the  
102 thermokarst lakes serve as significant carbon sources through carbon flux measurements in 163  
103 thermokarst lakes during the summer and autumn seasons. Wang et al. (2021) discovered that by  
104 comparing carbon fluxes in ten high-mountain ecosystems with different grassland types, these  
105 ecosystems act as sinks for carbon dioxide. The alpine meadows in the eastern QTP were identified  
106 as strong carbon sinks, with the highest annual average NEE recorded at  $-284 \text{ g C m}^{-2}$ . Forest  
107 ecosystems play a crucial role in the southeastern edge of the QTP, providing important support for  
108 climate regulation and forestry-based economic activities. Moreover, recent predictive studies  
109 suggest that under both current and future climate scenarios, the forested area in this region is  
110 expected to expand further, with coniferous forests continuing to grow into higher altitudes (Liu et  
111 al., 2021). Due to the extensive presence of permafrost in the QTP, forest net primary productivity  
112 exhibits a most pronounced response to surface temperatures in the continuous permafrost zone over  
113 multiple years. Therefore, the changes in permafrost in the QTP should not be overlooked, as they  
114 also have a significant impact on carbon absorption by forests (Mao et al., 2015). However, the QTP  
115 is a vast region with a widespread distribution of high-altitude and subalpine forests. Long-term  
116 monitoring is necessary to understand how these forests will respond to climate change.  
117 Furthermore, there is a significant data gap concerning the monitoring of carbon exchange capacity  
118 in the forests of the QTP, indicating the need for further data collection efforts. Based on this, we  
119 established a carbon flux monitoring site in the subalpine ecosystem of the Three Parallel Rivers  
120 Region, which is located on the southeastern edge of the QTP and is renowned as a global hotspot  
121 for biodiversity (Wang et al., 2022a). Our research objectives are to:

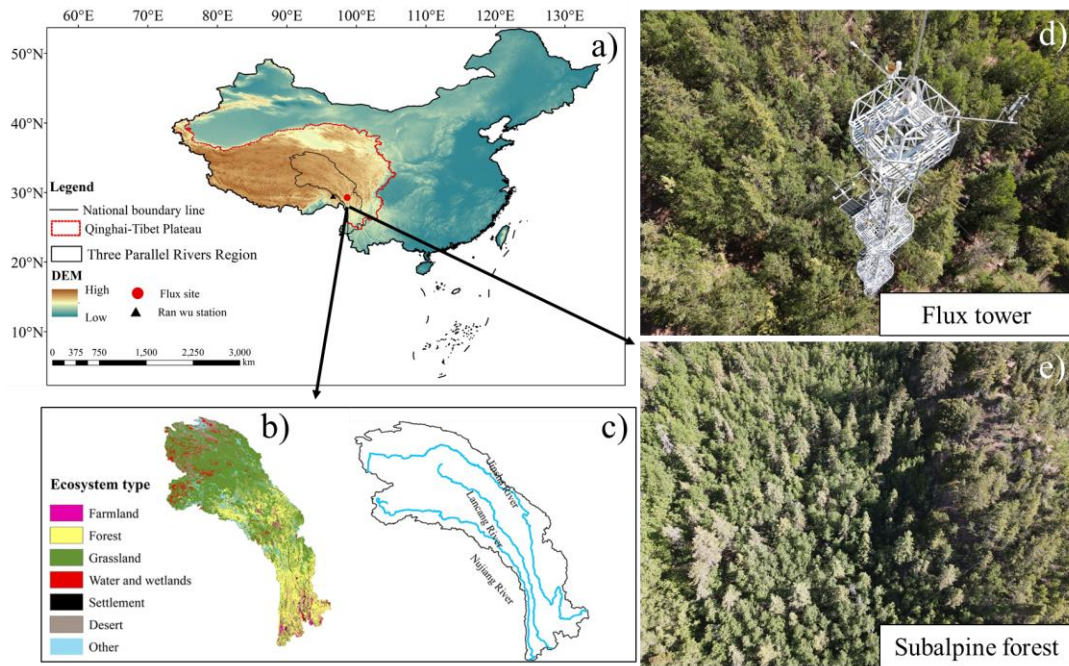
- 122 1) Determine whether the subalpine forests in the Three Parallel Rivers Region act as a carbon  
123 sink or source, and quantify the annual uptake or release of carbon dioxide;
- 124 2) Investigate the influences of main environmental factors on the carbon exchange process in the  
125 subalpine forests and identify the factors with the greatest impact, and;
- 126 3) Evaluate the carbon exchange capacity of subalpine forests in the QTP by comparing existing  
127 data with other ecosystems in the region.

128 This study will provide a data foundation and background support for accurately estimating  
129 the carbon balance of forests in high-altitude areas and for model simulations in the future.

130 **2 Materials and Methods**

131 2.1 Overview of the study site

132 The study site is located in the Hongla Mountain Yunnan Snub-nosed Monkey National Nature  
133 Reserve in Mangkang County, Tibet, China (29°17'10.78"N, 98°41'27.45"E), the core area of the  
134 watershed of the Three Parallel Rivers (Nujiang River, Lancang River, and Jinsha River). The  
135 elevation of the study site is 3755 m. The observation period was from November 2020 to October  
136 2022. The study area experiences large diurnal temperature variations and dry conditions in winter,  
137 while the summers are warm and humid. The average daily sunshine duration exceeds 10 h, with an  
138 annual average temperature of 5 °C and an average annual precipitation of around 600 mm within  
139 a year (Niu et al., 2023). The main tree species in the area include *Picea likiangensis* var. *rubescens*,  
140 *Abies squamata*, *Sabina tibetica* Kom, and *Abies ernestii*. They are accompanied by the growth of  
141 some *Quercus aquifolioides*, *Rhododendron lapponicum*, and *Potentilla fruticosa* shrubs. The  
142 average height of the trees is around 30 m, and the forest is in a relatively active growth phase,  
143 reaching the state of a mature forest. The vegetation coverage ranges from 70% to 80%. The  
144 dominant soil type is yellow-brown soil. The mountainous terrain contributes to distinct vertical  
145 climate characteristics and significant variations in water and heat conditions, with numerous dry  
146 and hot river valleys, widespread canyons, and a clear impact from the southwest and southeast  
147 monsoons. The varying elevations give rise to diverse ecosystems, transitioning from alpine forests  
148 to mountain shrubs. Above 4000 m asl, high alpine grasslands and meadows form a noticeable  
149 vegetation transition zone. The mountainous topography results in distinct vertical climate features  
150 and significant fluctuations in water and heat conditions, with precipitation showing a markedly  
151 uneven distribution throughout the study region (Zemin et al., 2023).



152

153 Figure 1. Location of the flux site (a). Ecosystem types (b) and main rivers (c) in the Three Parallel  
 154 Rivers Region. Flux tower (d) and forest top view (e). (The national boundary range in the figure  
 155 was retrieved from <http://bzdt.ch.mnr.gov.cn>, and elevation data and ecosystem type are from  
 156 [www.gscloud.cn](http://www.gscloud.cn).)

## 157 2.2 Eddy covariance system

158 **The EC system is deployed at a 35 m-high tower** located at the study site. At the top of the  
 159 tower, a 3-D wind velocity (Wind Master, Gill, UK) and an open-path infrared CO<sub>2</sub>/H<sub>2</sub>O analyzer  
 160 (LI-7500DS, Li-Cor, USA) were installed to measure CO<sub>2</sub> flux. The instruments had a measurement  
 161 frequency of 10 Hz. Additionally, micro-meteorological sensors were placed at different heights on  
 162 the tower, including sensors at 35 m for observing air temperature and humidity (HMP155A,  
 163 Vaisala, Finland), sensors at -5 cm for soil temperature (TEROS11, LI-Cor, USA), and sensors at  
 164 35 m for photosynthetically active radiation (LI-190R, LI-Cor, USA). **All data was stored for 30-**  
 165 **minute in** a SmartFlux 3 data logger (Li-Cor, USA) for future download.

## 166 2.3 Data processing and quality control

167 When considering only the turbulent transport of matter and energy in the vertical direction,  
 168 the carbon dioxide flux ( $F_c$ ) can be represented by the following equation (Yu and Sun, 2006;  
 169 Monteith et al., 1994):

170 
$$F_c = \overline{W'CO_2'} \quad (1)$$

171 Where  $W'$  is the vertical component of 3-D wind speed fluctuations ( $\text{m s}^{-1}$ ), and  $\text{CO}_2'$  represents the  
172 fluctuations in measured  $\text{CO}_2$  mole concentration. A positive  $F_c$  indicates carbon emissions, while  
173 a negative value represents carbon uptake.

174 The acquired 10 Hz raw data was processed and corrected using the EddyPro software  
175 (EddyPro 7.06, Li-Cor, USA). The calibration process involved outlier detection for flux data, lag  
176 elimination, coordinate rotation (Jia et al., 2020), ultrasonic temperature correction (Schotanus et  
177 al., 1983), frequency correction (Moncrieff et al., 1997), and Webb-Pearman-Leuning (WPL)  
178 correction (Leuning and King, 1992). After these controls, the integrity of the effective **FC raw data**  
179 we obtained reached 92.95 %. We removed outliers caused by environmental disturbances such as  
180 power outages, rain, snow, and dust particles that interfered with the instrument. Due to the slope of  
181 the underlying surface being around 5 degrees, we also corrected from non-uniform and non-flat  
182 surfaces using EddyPro for double-coordinate rotation (Cao et al., 2019). As a result, we obtained  
183 half-hourly flux data with associated data quality indicators. To evaluate the turbulence steadiness,  
184 we employed the "0-1-2" quality assessment method, which classified flux results into three quality  
185 levels: 0 for excellent data quality, 1 for moderate data quality, and 2 for low data quality (Mauder  
186 and Foken, 2011; Foken et al., 2005). We removed data points labeled with a quality level of "2".  
187 We further eliminated flux data with negative values during nighttime since plants do not perform  
188 photosynthesis at night. Additionally, we conducted spectral analysis to identify and remove data  
189 points with values significantly deviating from normal. Finally, friction velocities ( $u^*$ ) for each of  
190 the two years were determined separately using the method of moving point, and deleted data  
191 recorded during nighttime when  $u^*$  was less than 0.28 and 0.39  $\text{m s}^{-1}$  (Reichstein et al., 2005). After  
192 excluding outliers from the data, the data integrity is 72.67%. Tovi software (Tovi, Li-Cor, USA)  
193 was used in the process.

194 When turbulence is weak, a portion of  $\text{CO}_2$  is stored in the vegetation canopy and the  
195 atmosphere below the measurement height. At this time, the NEE is calculated as (Zhang et al.,  
196 2018):

$$197 \quad \text{NEE} = F_C + F_S \quad (2)$$

198 Where NEE represents the net ecosystem exchange of  $\text{CO}_2$ ,  $F_C$  stands for the observed flux during  
199 a specific period,  $F_S$  represents the  $\text{CO}_2$  storage in the forest canopy,  $F_S$  is calculated as  $(\Delta c/\Delta t) \cdot h$ ,



200 where  $\Delta c$  is the difference in CO<sub>2</sub> concentration between two consecutive measurements,  $\Delta t$  is the  
201 time interval between two consecutive measurements, and  $h$  is 35 m.

202 We adopted the following formula as a gap-filling strategy for daytime NEE ( $NEE_{day}$ )  
203 concerning PAR, aiming to address missing values during the daytime (Falge et al., 2001):

$$204 \quad NEE_{day} = \frac{a \times PAR \times P_{max}}{a \times PAR + P_{max}} - R_{day} \quad (3)$$

205 where  $a$  ( $\mu\text{mol CO}_2/\mu\text{mol PAR}$ ) represents the apparent photosynthetic quantum efficiency, which  
206 characterizes the maximum efficiency of converting light energy during photosynthesis; PAR ( $\mu\text{mol}$   
207  $\text{m}^{-2} \text{s}^{-1}$ ) is the photosynthetically active radiation, a measure of the amount of light energy available  
208 for photosynthesis;  $P_{max}$  ( $\mu\text{mol CO}_2 \text{ m}^{-2} \text{ s}^{-1}$ ) is the apparent maximum photosynthetic rate,  
209 representing the maximum CO<sub>2</sub> uptake rate under optimal conditions, and;  $R_{day}$  ( $\mu\text{mol CO}_2 \text{ m}^{-2} \text{ s}^{-1}$ )  
210 is the daytime dark respiration rate, which denotes the rate of CO<sub>2</sub> release during daylight hours.  $a$ ,  
211  $P_{max}$ , and  $R_{day}$  are obtained through the non-linear fitting of the Michaelis-Menten model to the  
212 observed data.

213 During the nighttime, the NEE is modeled using an exponential function of ecosystem  
214 respiration and soil temperature to fill in the missing values of NEE during the night ( $NEE_{night}$ )  
215 (Lloyd and Taylor, 1994; Kato et al., 2006):

$$216 \quad NEE_{night} = a \times \exp(bt) \quad (4)$$

217 Where  $a$  and  $b$  are estimated values for the exponential function used in modeling  $NEE_{night}$ , and;  $t$   
218 represents the soil temperature measured at the depth of 5 cm. Origin 2023 (Originlab Corporation,  
219 USA) is the data processing software used for this analysis. For the missing data, interpolation was  
220 performed using Tovi software allows for data interpolation to fill in the gaps and ensure a  
221 continuous dataset for further analysis (Reichstein et al., 2005). 27.33% of missing data were  
222 interpolated using Tovi after filtering, resulting in a flux data set with complete data integrity.

223 In flux analysis, the significance of source area contributions cannot be overlooked. In this  
224 study, the peak distances of the 90% flux contribution areas averaged over two years are 364.2 and  
225 357.1m, respectively. In terms of seasons, the average peak distances of the 90% flux contribution  
226 areas for winter, spring, summer, and autumn over the two years are as follows: 353.9, 358.2, 350.05,  
227 and 344.34m, respectively.

## 228 2.4 Flux partitioning

229 Ecosystem respiration (RE) is the sum of plant and heterotrophic respiration in an ecosystem  
230 and is obtained by adding the measured nighttime data to the extrapolated daytime data. Gross  
231 primary productivity (GPP) is the total amount of organic carbon fixed by green plants through  
232 photosynthesis per unit of time and per unit of area:

$$233 \quad RE = R_{\text{day}} + R_{\text{night}} \quad (5)$$

$$234 \quad GPP = -NEE + RE \quad (6)$$

235 Carbon use efficiency (CUE) is a crucial parameter that reflects the ability of an ecosystem to  
236 sequester carbon. It is defined as the ratio of net ecosystem productivity (NEP) to gross primary  
237 productivity. CUE can be expressed using the following equation:

$$238 \quad CUE = \frac{NEP}{GPP} = \frac{-NEE}{GPP} \quad (7)$$

239 To study the variation of ecosystem respiration rates with environmental factors, we considered  
240 the dependence of nocturnal ecosystem respiration on soil temperature (Pavelka et al., 2007;  
241 Mamkin et al., 2023):

$$242 \quad Q_{10} = \exp(10 \times \alpha) \quad (8)$$

$$243 \quad \ln(NEE_{\text{night}}) = \alpha \times T + \gamma \quad (9)$$

244 Where T is the soil temperature (°C) and  $\gamma$  is an empirical parameter of the equation.

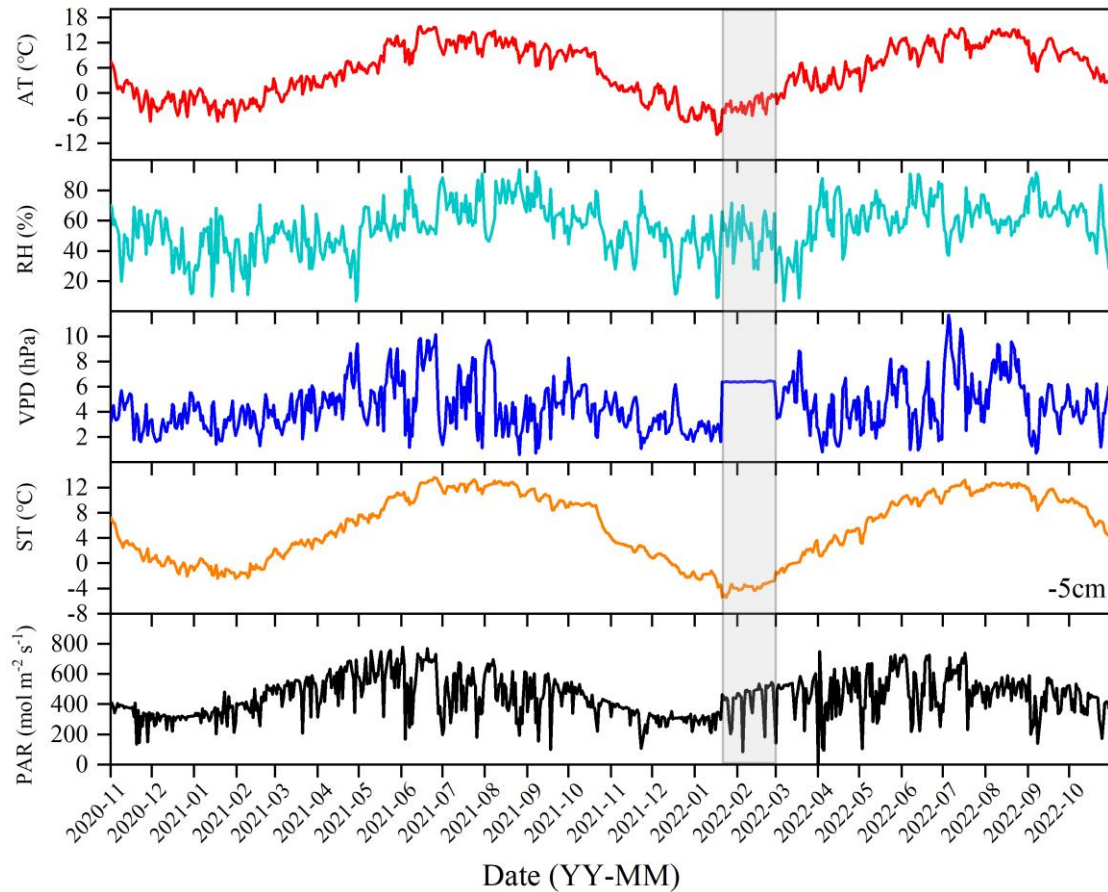
245 To clarify the carbon sink potential of forests in the QTP and to compare it with other  
246 ecosystems, a search was conducted in two authoritative databases, Web of Science and China  
247 National Knowledge Internet, for research articles on the current utilization of EC systems in the  
248 QTP. A total of 82 research results were collected from 48 studies, and their annual average  
249 environmental factors, such as air temperature, precipitation, and altitude, were obtained.

## 250 **3 Results**

### 251 3.1 Daily changes in main environmental factors

252 During the observational period, the environmental conditions exhibited significant  
253 fluctuations. The winter and spring seasons were characterized by cold and dry conditions, while  
254 the summer and autumn seasons were warm and humid. The daily maximum **AT** recorded was  
255 15.87 °C (on June 15, 2021), and the minimum temperature was -9.88 °C (on January 17, 2022),  
256 with a **mean annual** average of 5.5 °C over the two years. **RH** is averaged at 55.89%, and **VPD** is

257 averaged at 4.46 hPa. **ST** exhibited a similar trend to air temperature. The highest observed soil  
 258 temperature was 13.53 °C (on June 27, 2021), while the minimum was -3.78 °C (on January 18,  
 259 2022), with an annual average of 6.11 °C. **PAR** is averaged at 447.24 mol m<sup>-2</sup> s<sup>-1</sup>.

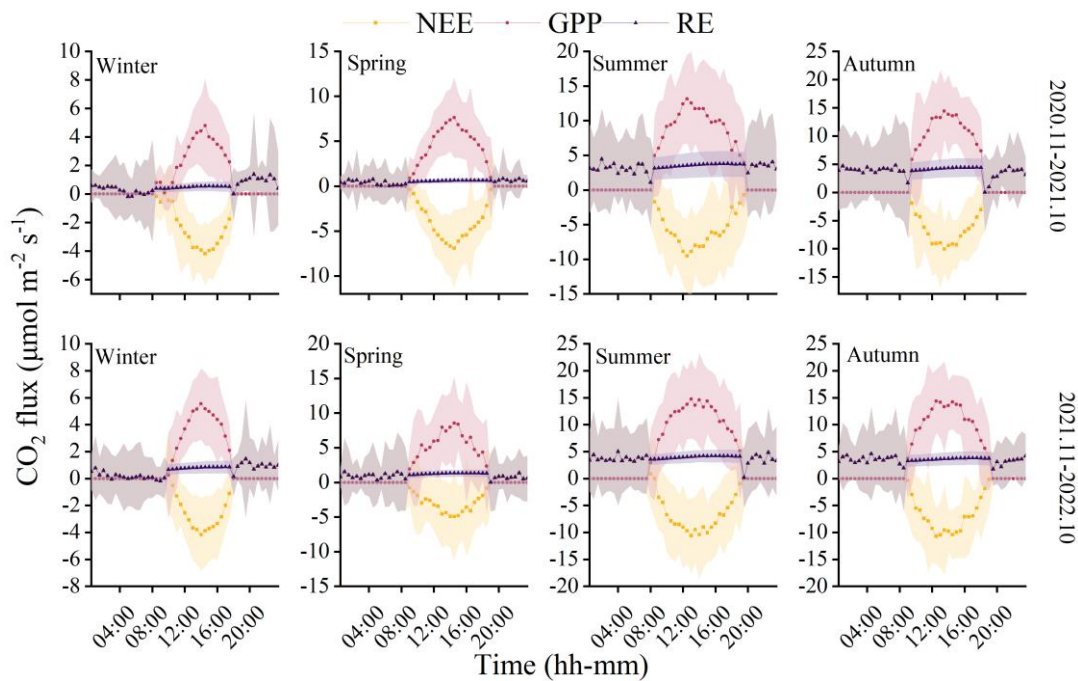


260  
 261 Figure 2. Daily values of main environmental factors, air temperature (AT), relative humidity (RH),  
 262 vapor pressure deficit (VPD), soil temperature (ST), and **photosynthetically** active radiation (PAR).  
 263 (The data of the shadow part in the figure comes from the Ranwu forest site (Figure 1). Since there  
 264 was no interpolated data source for VPD, the annual average was used instead.)

### 265 3.2 Seasonal dynamics of NEE, RE, and GPP

266 The observations from the forest ecosystem indicate distinct diurnal and seasonal variations in  
 267 NEE and GPP (Figure 3). The NEE and GPP exhibit a pronounced U-shaped curve, with significant  
 268 seasonal differences. The summer and autumn are characterized by peak carbon uptake, with the  
 269 maximum NEE reaching. During the nighttime, the ecosystem generally releases carbon, while  
 270 during favorable daytime meteorological conditions, it demonstrates a carbon uptake capacity. The  
 271 peak carbon absorption of the forest ecosystem occurs from 12:00 to 15:00 (Beijing time,  
 272 UTC+8:00). The daily carbon sequestration in summer and autumn is 1.5-3 hrs longer than in winter.

273 The timing of maximum carbon sequestration capacity changes with each season. In winter, the  
 274 transition from nighttime carbon release to daytime carbon uptake occurs around 08:30, which is  
 275 approximately 1 hour later than in summer. GPP characterizes the forest's carbon sequestration  
 276 capacity, and since photosynthesis does not occur at night, GPP is zero during nighttime. The  
 277 maximum daily total productivity is recorded at  $14.76 \pm 7.34 \mu\text{mol CO}_2 \text{ m}^{-2} \text{ s}^{-1}$  during the summer  
 278 of the second year, with a standard deviation indicating greater variability in GPP and NEE during  
 279 the summer and autumn compared to the winter and spring. Although diurnal variations in RE are  
 280 relatively small, there are significant seasonal differences. During the night, when only respiration  
 281 occurs, RE equals NEE. However, as photosynthesis becomes active during the day, RE gradually  
 282 increases and stabilizes. The respiratory rate of the coniferous forest is highest in autumn, being  
 283 eight times greater than in winter.

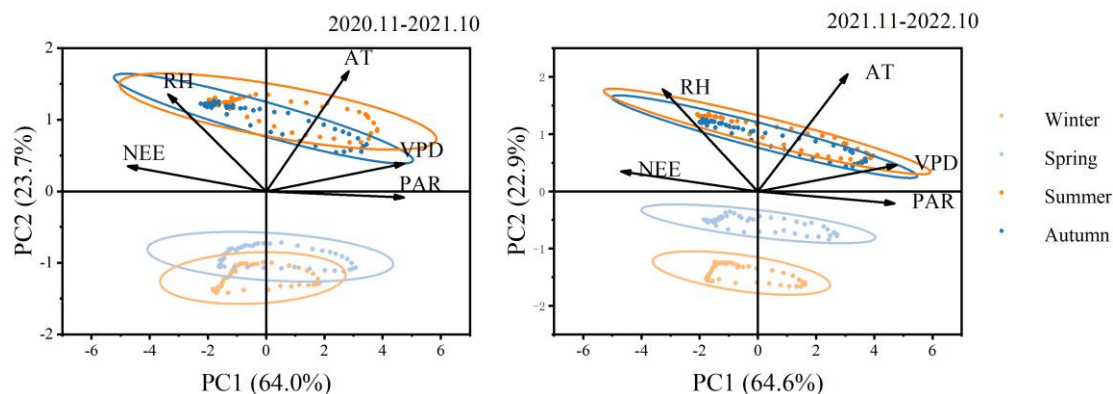


284  
 285 Figure 3. Monthly mean values of **CO<sub>2</sub> fluxes**

286 3.3 Relationship between NEE and main environmental factors

287 The PCA analysis of NEE and environmental factors (Figure 4) indicates that the explanations  
 288 for the first principal component (PC1) and the second principal component (PC2) are essentially  
 289 the same between the two years. The total contributions of PC1 and PC2 are 87.7% and 87.5%,  
 290 respectively, with PC1 accounting for 64.0% and 64.6% individually. The angle between  
 291 photosynthetically active radiation (PAR) and PC1 is minimal, suggesting a strong correlation

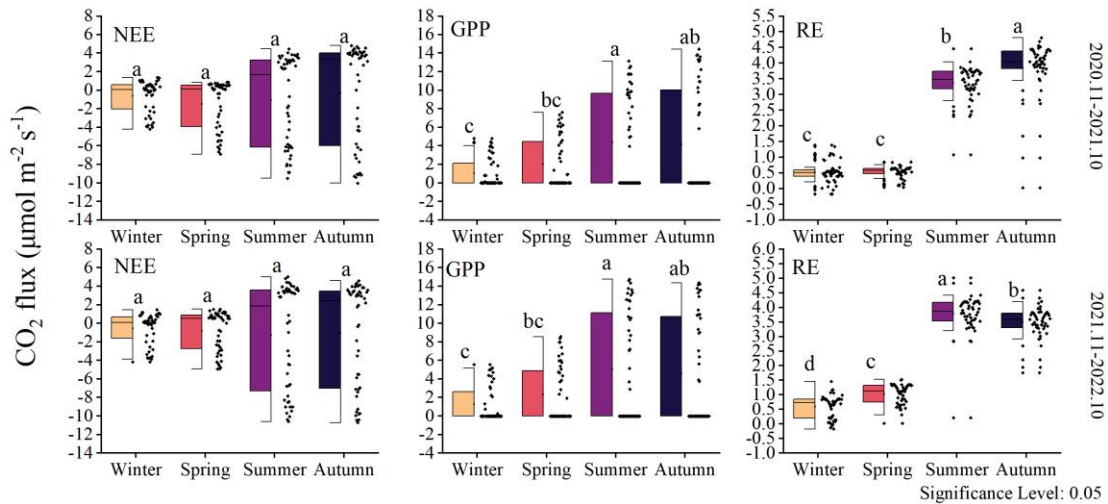
292 between PAR and PC1. Additionally, PAR and VPD contribute the most to PC1, while AT and RH  
 293 contribute the most to PC2. The analysis results reveal a significant positive correlation between  
 294 NEE and RH, while a significant negative correlation is observed with AT, VPD, and PAR.  
 295 **Increased RH is detrimental to forest carbon dioxide absorption. Excessively high relative humidity**  
 296 **causes plant leaf stomata to close, reducing the amount of carbon dioxide available to the plant. This,**  
 297 **in turn, leads to a decrease in the efficiency of carbon fixation through photosynthesis. Among these**  
 298 environmental factors, PAR plays a dominant role. Furthermore, the figure illustrates the  
 299 relationships between environmental factors, showing a positive correlation between RH and TA,  
 300 and a negative correlation with VPD and APR. The indicators exhibit some seasonality, with notable  
 301 differences between the winter-spring and summer-autumn seasons, indicating limited similarity  
 302 between seasons.



303  
 304 Figure 4. Principal component analysis of environmental factors and NEE

### 305 3.4 Seasonal variation of NEE, GPP, and RE

306 The NEE did not show significant inter-seasonal differences (Figure 5). However, data  
 307 distribution indicates that the variability in NEE rate differs across different seasons, particularly  
 308 between summer-autumn and winter-spring. The changes in GPP over the two years were similar,  
 309 with significant differences observed between summer and winter ( $P<0.05$ ). The RE was higher  
 310 during summer-autumn compared to winter-spring. The highest ecosystem respiration occurred in  
 311 the first year during autumn, while in the second year, it was highest during summer. Within the  
 312 same year, summer and autumn exhibited significant differences ( $P<0.05$ ), while between the same  
 313 seasons in different years, notable distinctions were not observed. This pattern is also reflected in  
 314 GPP and NEE.



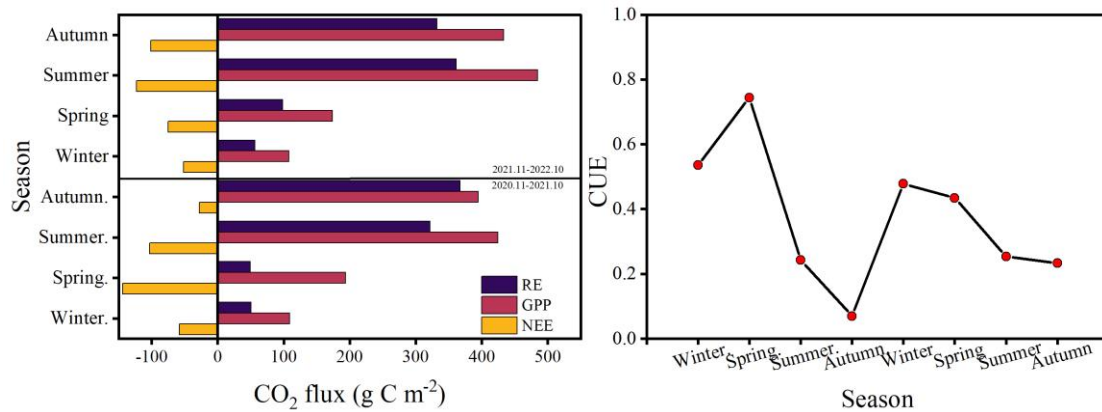
315

316

Figure 5. Seasonal variation of  $\text{CO}_2$  fluxes in two years

317 3.5 Changes in total NEE, GPP, RE, and CUE

318 The cumulative fluxes over the two years for the forest ecosystem are shown in Figure 6. NEE  
 319 indicates the net carbon sequestration in each month. The cumulative respiration reached its highest  
 320 value of  $361 \text{ g C m}^{-2}$  in the summer of 2022. The total NEE, GPP, and RE for the first year were  
 321  $-332$ ,  $1121$ , and  $788 \text{ g C m}^{-2}$ , respectively, and  $-351$ ,  $1199$ , and  $847 \text{ g C m}^{-2}$  for the second year,  
 322 respectively. The CUE was higher during the spring and lower during the autumn, with a maximum  
 323 value of  $0.74$  and a minimum value of  $0.07$ . The average CUE over the two years was  $0.40$  and  $0.35$ ,  
 324 respectively.



325

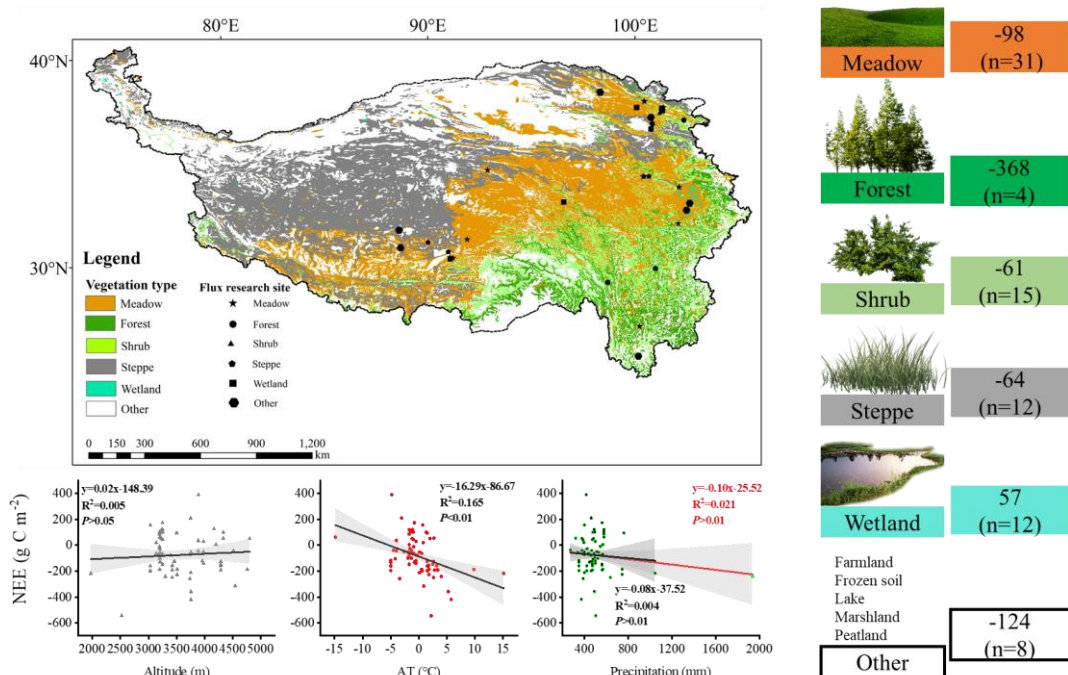
326

Figure 6. Change in total carbon flux and carbon use efficiency

327 3.6 The carbon sequestration potential of subalpine forests of QTP

328 To clarify the carbon sequestration contribution of the subalpine forests found in the QTP, we  
 329 compared these research results (Figure 7). Found that ecosystems with high vegetation cover

330 exhibited higher annual cumulative carbon sequestration. Among these ecosystems, the subalpine  
 331 forests in the QTP showed the highest carbon sequestration potential, reaching an average of 368 g  
 332 C m<sup>-2</sup> per year. The carbon sequestration potential of different ecosystems ranked as follows: forest >  
 333 meadow > steppe > shrub. The average value for wetlands indicated that they are a significant source  
 334 of CO<sub>2</sub>, releasing 57 g C m<sup>-2</sup> into the atmosphere annually. We also analyzed the influence of altitude,  
 335 mean annual air temperature, and precipitation on NEE at these sites in the QTP. It has been  
 336 observed that these sites cover a wide range of altitudes, ranging from 1977 to 4800 m. According  
 337 to existing results, an increase in elevation may lead to a reduction in carbon uptake, while the range  
 338 of mean annual temperature varies between -14.8 to 15.1 °C, and higher mean annual temperatures  
 339 significantly increase carbon uptake. Forests exhibit the highest mean annual precipitation,  
 340 averaging 827 mm, with mean annual precipitation having a relatively weak impact on the NEE.  
 341 These findings highlight the important role of subalpine forests in carbon sequestration in the QTP  
 342 and provide insights into the factors that affect carbon exchange in the QTP, such as altitude,  
 343 temperature, and precipitation.



344  
 345 Figure 7. Carbon exchange potential of different ecosystems in the Qinghai-Tibet Plateau

346 **4 Discussion**

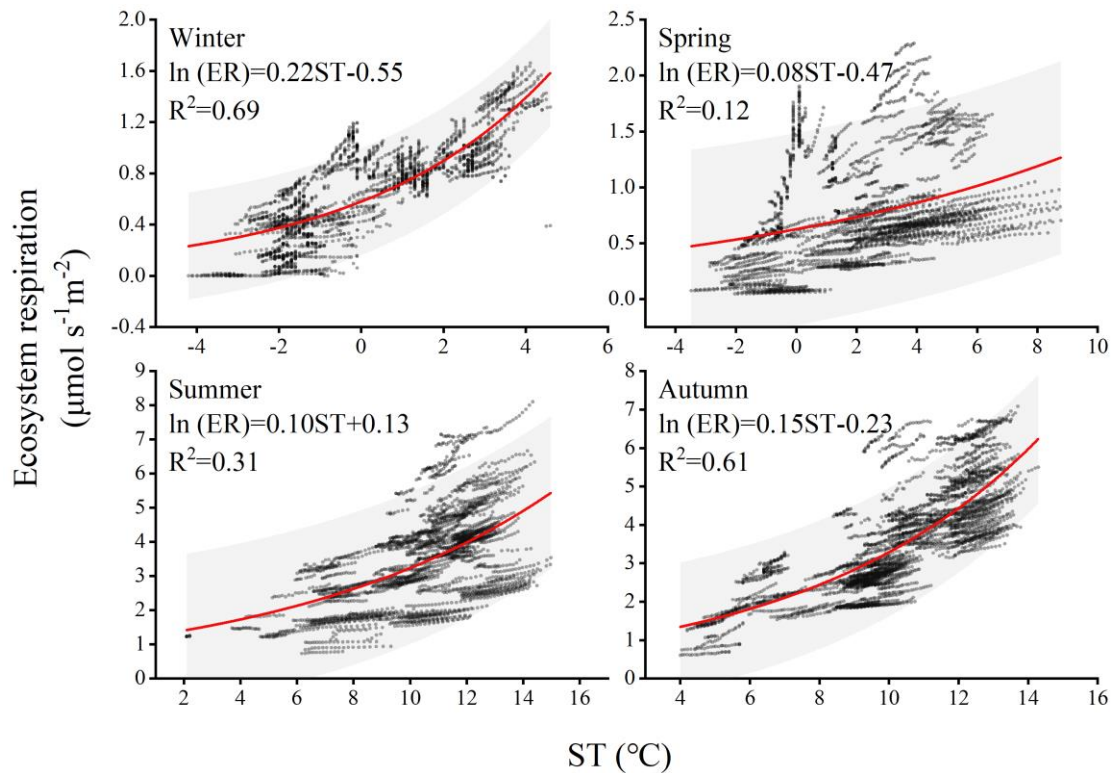
347 4.1 Main factors affecting the carbon sequestration function of subalpine forests

348 Climate change significantly affects the vegetation's carbon sequestration capacity, particularly  
349 at the seasonal scale due to phenological changes (Acosta-Hernández et al., 2020). In the short term,  
350 PAR, AT, RH, and VPD play important roles in regulating vegetation photosynthesis and,  
351 consequently, carbon uptake. For instance, PAR represents the portion of solar energy that can be  
352 utilized by plants and is an essential component in chloroplast reactions. PAR drives a nonlinear  
353 response of GPP to Solar-induced fluorescence (SIF) across different seasons, resulting in a strong  
354 positive correlation between GPP and SIF (Wang et al., 2023b). VPD affects photosynthesis and  
355 transpiration of leaves, with stomata serving as tiny pores mediating carbon dioxide uptake.  
356 Research has demonstrated that excessive increases in VPD are detrimental to photosynthesis. For  
357 instance, a moderate increase in VPD significantly reduces photosynthetic efficiency under light  
358 fluctuations, due to changes in RH and/or AT often accompanying fluctuations in light, studies also  
359 indicate that the impact of VPD on sunlight utilization efficiency is primarily determined by relative  
360 RH rather than AT (Liu et al., 2024). In different seasons, the same influencing factors exhibit  
361 varying degrees of contribution to NEE. For example, during winter, when the climatic conditions  
362 are relatively harsh with low air temperature and humidity, the forest maintains a low level of carbon  
363 uptake. On longer time scales, such as annual and decadal variations, the inherent changes in forest  
364 NEE may be attributed to disturbances and recovery (Hayek et al., 2018). In this study, significant  
365 differences in ecosystem respiration were observed during the summer and autumn in different years.  
366 Previous studies suggested that due to leaf aging or water stress, the photosynthetic light use  
367 efficiency of the ecosystem peaks after spring leaf expansion and gradually declines (Wehr et al.,  
368 2016). This implies a peak in carbon exchange during the summer, followed by higher productivity  
369 and ecosystem respiration in the following seasons. The variation in different years may be  
370 attributed to rainfall regulating the availability of natural resources such as water, biomass, litter,  
371 and soil nutrients (Schwinning and Sala, 2004). For instance, in temperate forests, when microbial  
372 biomass undergoes seasonal changes, microbial activity exhibits a seasonal lag in response to  
373 temperature variation, resulting in a seasonally delayed effect between litter heterotrophic  
374 respiration and temperature (Ataka et al., 2020). Whether such differences persist between different  
375 years on longer time scales remains to be demonstrated through more sustained and detailed  
376 research in the future. Ecosystem respiration sensitivity to temperature is represented by the  $Q_{10}$



377 coefficient. In this study, seasonal variations influenced the magnitude of  $Q_{10}$  (as shown in Figure  
378 8). The calculated  $Q_{10}$  for each season are as follows: 9.03, 2.22, 2.71, and 4.48. The winter season  
379 exhibited the highest sensitivity of forest ecosystem respiration to temperature, indicating that  
380 respiration rates in the winter are more responsive to changes in temperature compared to other  
381 seasons. The main reason for such differences is that ecosystem respiration consists of heterotrophic  
382 respiration and autotrophic respiration, which are typically governed by different factors (Edwards,  
383 1975). For instance, the high activity of soil microbes contributes to heterotrophic respiration, a  
384 process dominated by soil temperature and moisture conditions, which are severely restricted during  
385 the cold and dry conditions of winter (Falge et al., 2002). Simultaneously, due to the changing  
386 relative roles of growth and maintenance respiration, the allocation of autotrophic respiration varies  
387 seasonally. In winter, soil  $CO_2$  emissions constitute a significant portion of ecosystem  $CO_2$   
388 emissions, and in some boreal forests, the ratio between the two can reach 0.6 or even higher  
389 (Davidson et al., 2006). In winter, under the frequent coverage of snow, cold-adapted  
390 microorganisms thriving in a relatively narrow sub-zero temperature range engage in respiration  
391 and exhibit relatively high sensitivity to warming or cooling beyond this range (Monson et al., 2006).  
392 The seasonal patterns of the  $Q_{10}$  value are jointly determined by the variation in the ratio of soil  
393 respiration to ecosystem respiration, reflecting these seasonal changes.

394 Our integrated analysis (as shown in Figure 7) reveals that despite the high elevation of the  
395 "Third Pole", the topographic factor of elevation does not have a significant impact on carbon uptake.  
396 Instead, NEE gradually increases with a steep rise in elevation. Research conducted by Wang et al.  
397 (2023c) has indicated that mean annual average temperature and precipitation are the main driving  
398 factors of interannual variations in NEE in alpine meadows and alpine steppes. Decreased  
399 precipitation resulted in a transition into carbon sources in some regions with high precipitation-  
400 dependent alpine grasslands. It is worth noting that, among all data collection sites, alpine wetlands  
401 show an average carbon source trend. Due to prolonged flooding and low temperatures, microbial  
402 activity in alpine wetlands is hindered, and the accumulation of organic carbon from plant litter  
403 decomposition is substantial. As a result, approximately  $57 \text{ g C m}^{-2}$  is emitted into the atmosphere  
404 annually. Previous studies have indicated that NEE in alpine wetlands is increasing with global  
405 warming (Yasin et al., 2022).



406

407

Figure 8. Relationship between NEE night and soil temperature in different seasons

408

#### 4.2 Sustained carbon sequestration of subalpine forests

409

410

411

412

413

414

415

416

417

418

419

420

421

422

423

Subalpine forests are integral components of global alpine ecosystems and play crucial roles in the global carbon cycle. Our study on subalpine forests demonstrates a continuous **absorption** of carbon dioxide even during winter, which aligns well with measurements taken in the vicinity of Mount Fuji in Japan (Mizoguchi et al., 2012). The age of subalpine forests is a crucial factor influencing sustained carbon sequestration. Based on NPP simulations of natural subalpine forests in the Northern Rockies, Carey (2001) found that aboveground net primary productivity reaches its maximum after approximately 250 years, followed by a decline, this challenges the previous view that forests older than 100 years are generally considered to be unimportant carbon sinks. Compared to the forest (mature forest) of Mount Gongga in the QTP (e.g., Zhang et al., 2018), the subalpine forest in this study exhibits a stronger carbon sequestration capacity. However, its carbon sequestration ability is slightly weaker than that of the Qilian Mountains high-mountain forests (approximately 60-70 years old) in the QTP (Zhang et al., 2018; Du et al., 2022b). Although existing flux monitoring results of high-altitude forests in the QTP indicate that these forest ecosystems act as carbon sinks, it is important to consider that globally there are still many cold regions with coniferous forests **servicing** as carbon sources. For example, continuous  $\text{CO}_2$  flux monitoring from

424 native boreal forests in Sweden for over 10 years indicates that they are a net carbon source, which  
425 is attributed to the contribution of woody debris to RE due to disturbances such as extreme weather  
426 events, fires, insect infestations, and pathogen attacks (Hadden and Grelle, 2017). In the summer of  
427 2018, Europe experienced a heatwave that affected the carbon cycling in forests. The mixed  
428 coniferous-deciduous forest in southern Estonian, under the influence of the heatwave, transitioned  
429 from a net carbon sink to a net carbon source in 2018 (Krasnova et al., 2022). Particular attention  
430 should be paid to the long-term monitoring in high-altitude environments of the impact of  
431 disturbances on forest carbon sequestration capacity. Our study has shown that forests in the QTP  
432 have the strongest carbon sink capacity, indicating that alpine forests will have an important  
433 sustained effect on carbon reduction in the QTP in the context of future climate change, but whether  
434 this sustained effect will be longer than other ecosystems is still unknown. However, a modeling  
435 experiment in a large semi-arid area of California predicted that grasslands are more resilient carbon  
436 sinks than forests in responding to climate change in the 21st century (Dass et al., 2018). In terms  
437 of carbon sequestration rate, forests in the QTP were significantly stronger than other ecosystems,  
438 followed by grasslands, while alpine deserts and alpine grasslands in the north-western and southern  
439 regions were the main carbon sources (Wu et al., 2022). Forests are mostly distributed in the south-  
440 eastern margin of the QTP and the mid-altitude area near 3000 m in the Sichuan-Tibet alpine gorge  
441 area, with an area of  $19.3 \times 10^4 \text{ km}^2$  (Wang et al., 2022b). Based on the average value of a few  
442 current carbon flux monitoring, the forest in the QTP will absorb about  $71 \times 10^6 \text{ Mg C year}^{-1}$ .

## 443 **5 Conclusion**

444 This study explores the carbon sequestration function, seasonal variations, and climate drivers  
445 of subalpine forests in the QTP. Over the observational period, we synchronously monitored  
446 ecosystem carbon exchange and primary environmental factors using an eddy covariance system.  
447 **The research reveals that the subalpine forest acts as a carbon sink. Over the two years, the total**  
448 **NEE, GPP, and RE were  $-332$ ,  $1121$ , and  $788 \text{ g C m}^{-2}$  in first year, and  $-351$ ,  $1199$ , and  $847 \text{ g C m}^{-2}$**   
449 **in second year.** Photosynthetically active radiation was identified as the primary control of NEE,  
450 **Relative humidity is negatively correlated with NEE, and its increase is not conducive to carbon**  
451 **sink. NEE reached its peak in autumn. Combining results from other eddy covariance sites on the**  
452 **QTP, this study highlights that forests have the highest carbon sequestration potential, reaching 368**

453 g C m<sup>-2</sup> annually, followed by meadows (-98 g C m<sup>-2</sup>), steppes (-64 g C m<sup>-2</sup>), and shrubs (-61 g C  
454 m<sup>-2</sup>). In contrast, wetlands were identified as a significant source of carbon dioxide (57 g C m<sup>-2</sup>).  
455 Despite the challenges posed by climate change, the subalpine forests in the QTP retain substantial  
456 carbon sequestration potential. Strengthening conservation and management efforts for subalpine  
457 forests is crucial to ensure their continued and significant carbon sequestration function in the future.  
458 Overall, this research underscores the vital role of subalpine forests in the QTP as essential carbon  
459 sink regions, playing a critical role in the context of global climate change.

460 **Data availability.** The data is available from the authors on request.

461 **Authorship contributions.** **Niu Zhu:** Conceptualization, study design, data analyses,  
462 visualization, writing-original draft. **JinNiu Wang:** study design, writing—review & editing,  
463 supervision, project administration, funding acquisition. **Dongliang Luo and Xufeng Wang:**  
464 writing-reviewing & editing. **Cheng Shen and Ning Wu:** resources, data curation, supervision. all  
465 authors approved the final manuscript.

466 **Declaration of competing interest.** The authors declare that they have no conflict of interest.

467 **Acknowledgements.** We thank Ms. Neha Bisht for her substantial comments and language  
468 revision to improve the manuscript. This study was funded by CAS "Light of West China" Program  
469 (2021XBZG-XBQNXX-A-007); The National Natural Science Foundation of China (31971436);  
470 The State Key Laboratory of Cryospheric Science, Northwest Institute of Eco-Environment and  
471 Resources, Chinese Academy Sciences (SKLCS-OP-2021-06).

## 472 **Reference**

473 Acosta-Hernández, A. C., Padilla-Martínez, J. R., Hernández-Díaz, J. C., Prieto-Ruiz, J. A., Goche-  
474 Telles, J. R., Nájera-Luna, J. A., and Pompa-García, M.: Influence of Climate on Carbon  
475 Sequestration in Conifers Growing under Contrasting Hydro-Climatic Conditions, *Forests*, 11, 1134,  
476 2020.

477 Ataka, M., Kominami, Y., Sato, K., and Yoshimura, K.: Microbial Biomass Drives Seasonal  
478 Hysteresis in Litter Heterotrophic Respiration in Relation to Temperature in a Warm-Temperate  
479 Forest, *Journal of Geophysical Research: Biogeosciences*, 125, e2020JG005729,  
480 <https://doi.org/10.1029/2020JG005729>, 2020.

481 Banbury Morgan, R., Herrmann, V., Kunert, N., Bond-Lamberty, B., Muller-Landau, H. C., and

482 Anderson-Teixeira, K. J.: Global patterns of forest autotrophic carbon fluxes, *Global Change*  
483 *Biology*, 27, 2840-2855, <https://doi.org/10.1111/gcb.15574>, 2021.

484 Baumgartner, S., Barthel, M., Drake, T. W., Bauters, M., Makelele, I. A., Mugula, J. K., Summerauer,  
485 L., Gallarotti, N., Cizungu Ntaboba, L., Van Oost, K., Boeckx, P., Doetterl, S., Werner, R. A., and  
486 Six, J.: Seasonality, drivers, and isotopic composition of soil CO<sub>2</sub> fluxes from tropical forests of the  
487 Congo Basin, *Biogeosciences*, 17, 6207-6218, [10.5194/bg-17-6207-2020](https://doi.org/10.5194/bg-17-6207-2020), 2020.

488 Cai, W., He, N., Li, M., Xu, L., Wang, L., Zhu, J., Zeng, N., Yan, P., Si, G., and Zhang, X.: Carbon  
489 sequestration of Chinese forests from 2010 to 2060: Spatiotemporal dynamics and its regulatory  
490 strategies, *Science Bulletin*, 67, 836-843, 2022.

491 Cao, S., Cao, G., Chen, K., Han, G., Liu, Y., Yang, Y., and Li, X.: Characteristics of CO<sub>2</sub>, water  
492 vapor, and energy exchanges at a headwater wetland ecosystem of the Qinghai Lake, *Canadian*  
493 *Journal of Soil Science*, 99, 227-243, [10.1139/cjss-2018-0104](https://doi.org/10.1139/cjss-2018-0104), 2019.

494 Carey, E. V., Sala, A., Keane, R., and Callaway, R. M.: Are old forests underestimated as global  
495 carbon sinks?, *Global Change Biology*, 7, 339-344, [10.1046/j.1365-2486.2001.00418.x](https://doi.org/10.1046/j.1365-2486.2001.00418.x), 2001.

496 Chen, H., Ju, P. J., Zhu, Q., Xu, X. L., Wu, N., Gao, Y. H., Feng, X. J., Tian, J. Q., Niu, S. L., Zhang,  
497 Y. J., Peng, C. H., and Wang, Y. F.: Carbon and nitrogen cycling on the Qinghai-Tibetan Plateau,  
498 *NATURE REVIEWS EARTH & ENVIRONMENT*, 3, 701-716, [10.1038/s43017-022-00344-2](https://doi.org/10.1038/s43017-022-00344-2),  
499 2022.

500 Cole, J. J., Caraco, N. F., Kling, G. W., and Kratz, T. K.: Carbon dioxide supersaturation in the  
501 surface waters of lakes, *Science*, 265, 1568-1570, 1994.

502 Dass, P., Houlton, B. Z., Wang, Y., and Warlind, D.: Grasslands may be more reliable carbon sinks  
503 than forests in California, *Environmental Research Letters*, 13, 074027, [10.1088/1748-9326/aacb39](https://doi.org/10.1088/1748-9326/aacb39),  
504 2018.

505 Davidson, E. A., Richardson, A. D., Savage, K. E., and Hollinger, D. Y.: A distinct seasonal pattern  
506 of the ratio of soil respiration to total ecosystem respiration in a spruce-dominated forest, *Global*  
507 *Change Biology*, 12, 230-239, <https://doi.org/10.1111/j.1365-2486.2005.01062.x>, 2006.

508 Du, C., Zhou, G., and Gao, Y.: Grazing exclusion alters carbon flux of alpine meadow in the Tibetan  
509 Plateau, *Agricultural and Forest Meteorology*, 314, 108774, 2022a.

510 Du, Y., Pei, W., Zhou, H., Li, J., Wang, Y., and Chen, K.: Net ecosystem exchange of carbon dioxide

511 fluxes and its driving mechanism in the forests on the Tibetan Plateau, *Biochemical Systematics and*  
512 *Ecology*, 103, 10.1016/j.bse.2022.104451, 2022b.

513 Ebermayer, E.: Die gesammte Lehre der Waldstreu mit Rücksicht auf die chemische Statik des  
514 Waldbaues: unter Zugrundlegung der in den Königl. Staatsforsten Bayerns angestellten  
515 Untersuchungen, Springer 1876.

516 Edwards, N. T.: Effects of Temperature and Moisture on Carbon Dioxide Evolution in a Mixed  
517 Deciduous Forest Floor, *Soil Science Society of America Journal*, 39, 361-365,  
518 <https://doi.org/10.2136/sssaj1975.03615995003900020034x>, 1975.

519 Falge, E., Baldocchi, D., Tenhunen, J., Aubinet, M., Bakwin, P., Berbigier, P., Bernhofer, C., Burba,  
520 G., Clement, R., Davis, K. J., Elbers, J. A., Goldstein, A. H., Grelle, A., Granier, A., Guðmundsson,  
521 J., Hollinger, D., Kowalski, A. S., Katul, G., Law, B. E., Malhi, Y., Meyers, T., Monson, R. K.,  
522 Munger, J. W., Oechel, W., Paw U, K. T., Pilegaard, K., Rannik, Ü., Rebmann, C., Suyker, A.,  
523 Valentini, R., Wilson, K., and Wofsy, S.: Seasonality of ecosystem respiration and gross primary  
524 production as derived from FLUXNET measurements, *Agricultural and Forest Meteorology*, 113,  
525 53-74, [https://doi.org/10.1016/S0168-1923\(02\)00102-8](https://doi.org/10.1016/S0168-1923(02)00102-8), 2002.

526 Falge, E., Baldocchi, D., Olson, R., Anthoni, P., Aubinet, M., Bernhofer, C., Burba, G., Ceulemans,  
527 R., Clement, R., Dolman, H., Granier, A., Gross, P., Grünwald, T., Hollinger, D., Jensen, N.-O.,  
528 Katul, G., Keronen, P., Kowalski, A., Lai, C. T., Law, B. E., Meyers, T., Moncrieff, J., Moors, E.,  
529 Munger, J. W., Pilegaard, K., Rannik, Ü., Rebmann, C., Suyker, A., Tenhunen, J., Tu, K., Verma, S.,  
530 Vesala, T., Wilson, K., and Wofsy, S.: Gap filling strategies for defensible annual sums of net  
531 ecosystem exchange, *Agricultural and Forest Meteorology*, 107, 43-69,  
532 [https://doi.org/10.1016/S0168-1923\(00\)00225-2](https://doi.org/10.1016/S0168-1923(00)00225-2), 2001.

533 Foken, T., Göckede, M., Mauder, M., Mahrt, L., Amiro, B., and Munger, W.: Post-Field Data  
534 Quality Control, in: *Handbook of Micrometeorology: A Guide for Surface Flux Measurement and*  
535 *Analysis*, edited by: Lee, X., Massman, W., and Law, B., Springer Netherlands, Dordrecht, 181-208,  
536 10.1007/1-4020-2265-4\_9, 2005.

537 Hadden, D. and Grelle, A.: Net CO<sub>2</sub> emissions from a primary boreo-nemoral forest over a 10 year  
538 period, *Forest Ecology and Management*, 398, 164-173,  
539 <https://doi.org/10.1016/j.foreco.2017.05.008>, 2017.

540 Hayek, M. N., Longo, M., Wu, J., Smith, M. N., Restrepo-Coupe, N., Tapajos, R., da Silva, R.,  
541 Fitzjarrald, D. R., Camargo, P. B., Hutyrá, L. R., Alves, L. F., Daube, B., Munger, J. W., Wiedemann,  
542 K. T., Saleska, S. R., and Wofsy, S. C.: Carbon exchange in an Amazon forest: from hours to years,  
543 *Biogeosciences*, 15, 4833-4848, 10.5194/bg-15-4833-2018, 2018.

544 Jia, X., Mu, Y., Zha, T., Wang, B., Qin, S., and Tian, Y.: Seasonal and interannual variations in  
545 ecosystem respiration in relation to temperature, moisture, and productivity in a temperate semi-  
546 arid shrubland, *Science of The Total Environment*, 709, 136210,  
547 <https://doi.org/10.1016/j.scitotenv.2019.136210>, 2020.

548 KATO, T., TANG, Y., GU, S., HIROTA, M., DU, M., LI, Y., and ZHAO, X.: Temperature and  
549 biomass influences on interannual changes in CO<sub>2</sub> exchange in an alpine meadow on the Qinghai-  
550 Tibetan Plateau, *Global Change Biology*, 12, 1285-1298, <https://doi.org/10.1111/j.1365->  
551 [2486.2006.01153.x](https://doi.org/10.1111/j.1365-2486.2006.01153.x), 2006.

552 Kondo, M., Saitoh, T. M., Sato, H., and Ichii, K.: Comprehensive synthesis of spatial variability in  
553 carbon flux across monsoon Asian forests, *Agricultural and Forest Meteorology*, 232, 623-634, 2017.

554 Konopka, J., Heusinger, J., and Weber, S.: Extensive Urban Green Roof Shows Consistent Annual  
555 Net Uptake of Carbon as Documented by 5 Years of Eddy-Covariance Flux Measurements, *Journal*  
556 *of Geophysical Research: Biogeosciences*, 126, e2020JG005879, 2021.

557 Krasnova, A., Mander, Ü., Noe, S. M., Uri, V., Krasnov, D., and Soosaar, K.: Hemiboreal forests'  
558 CO<sub>2</sub> fluxes response to the European 2018 heatwave, *Agricultural and Forest Meteorology*, 323,  
559 109042, <https://doi.org/10.1016/j.agrformet.2022.109042>, 2022.

560 Landsberg, J. and Waring, R.: A generalised model of forest productivity using simplified concepts  
561 of radiation-use efficiency, carbon balance and partitioning, *Forest ecology and management*, 95,  
562 209-228, 1997.

563 Laurin, G. V., Chen, Q., Lindsell, J. A., Coomes, D. A., Del Frate, F., Guerriero, L., Pirotti, F., and  
564 Valentini, R.: Above ground biomass estimation in an African tropical forest with lidar and  
565 hyperspectral data, *ISPRS Journal of Photogrammetry and Remote Sensing*, 89, 49-58, 2014.

566 Leuning, R. and King, K. M.: Comparison of eddy-covariance measurements of CO<sub>2</sub> fluxes by  
567 open- and closed-path CO<sub>2</sub> analysers, *Boundary-Layer Meteorology*, 59, 297-311,  
568 10.1007/BF00119818, 1992.

569 Li, L., Zhang, Y., Wu, J., Li, S., Zhang, B., Zu, J., Zhang, H., Ding, M., and Paudel, B.: Increasing  
570 sensitivity of alpine grasslands to climate variability along an elevational gradient on the Qinghai-  
571 Tibet Plateau, *Science of the Total Environment*, 678, 21-29, 2019.

572 Li, X. Y., Shi, F. Z., Ma, Y. J., Zhao, S. J., and Wei, J. Q.: Significant winter CO<sub>2</sub> uptake by saline  
573 lakes on the Qinghai-Tibet Plateau, *Global Change Biology*, 28, 2041-2052, 2022.

574 Liu, C., Wu, Z., Hu, Z., Yin, N., Islam, A. T., and Wei, Z.: Characteristics and influencing factors of  
575 carbon fluxes in winter wheat fields under elevated CO<sub>2</sub> concentration, *Environmental Pollution*,  
576 307, 119480, 2022.

577 Liu, J., Zou, H.-X., Bachelot, B., Dong, T., Zhu, Z., Liao, Y., Plenković-Moraj, A., and Wu, Y.:  
578 Predicting the responses of subalpine forest landscape dynamics to climate change on the eastern  
579 Tibetan Plateau, *Global Change Biology*, 27, 4352-4366, <https://doi.org/10.1111/gcb.15727>, 2021.

580 Liu, N.-Y., Yang, Q.-Y., Wang, J.-H., Zhang, S.-B., Yang, Y.-J., and Huang, W.: Differential Effects  
581 of Increasing Vapor Pressure Deficit on Photosynthesis at Steady State and Fluctuating Light,  
582 *Journal of Plant Growth Regulation*, 10.1007/s00344-024-11268-0, 2024.

583 Lloyd, J. and Taylor, J. A.: On the temperature dependence of soil respiration, *Functional Ecology*,  
584 8, 315-323, 1994.

585 Mamkin, V., Avilov, V., Ivanov, D., Varlagin, A., and Kurbatova, J.: Interannual variability in the  
586 ecosystem CO<sub>2</sub> fluxes at a paludified spruce forest and ombrotrophic bog in the southern taiga,  
587 *Atmospheric Chemistry and Physics*, 23, 2273-2291, 10.5194/acp-23-2273-2023, 2023.

588 Mao, D., Luo, L., Wang, Z., Zhang, C., and Ren, C.: Variations in net primary productivity and its  
589 relationships with warming climate in the permafrost zone of the Tibetan Plateau, *Journal of*  
590 *Geographical Sciences*, 25, 967-977, 10.1007/s11442-015-1213-8, 2015.

591 Mauder, M. and Foken, T.: Documentation and Instruction Manual of the Eddy-Covariance  
592 Software Package TK3 (update),

593 Mizoguchi, Y., Ohtani, Y., Takanashi, S., Iwata, H., Yasuda, Y., and Nakai, Y.: Seasonal and  
594 interannual variation in net ecosystem production of an evergreen needleleaf forest in Japan, *Journal*  
595 *of Forest Research*, 17, 283-295, 10.1007/s10310-011-0307-0, 2012.

596 Moncrieff, J. B., Massheder, J. M., de Bruin, H., Elbers, J., Friborg, T., Heusinkveld, B., Kabat, P.,  
597 Scott, S., Soegaard, H., and Verhoef, A.: A system to measure surface fluxes of momentum, sensible



598 heat, water vapour and carbon dioxide, *Journal of Hydrology*, 188-189, 589-611,  
599 [https://doi.org/10.1016/S0022-1694\(96\)03194-0](https://doi.org/10.1016/S0022-1694(96)03194-0), 1997.

600 Monson, R. K., Lipson, D. L., Burns, S. P., Turnipseed, A. A., Delany, A. C., Williams, M. W., and  
601 Schmidt, S. K.: Winter forest soil respiration controlled by climate and microbial community  
602 composition, *Nature*, 439, 711-714, 10.1038/nature04555, 2006.

603 Monteith, J. L., Unsworth, M. H., and Webb, A.: Principles of environmental physics, *Quarterly*  
604 *Journal of the Royal Meteorological Society*, 120, 1699, 1994.

605 Mu, C., Mu, M., Wu, X., Jia, L., Fan, C., Peng, X., Ping, C. I., Wu, Q., Xiao, C., and Liu, J.: High  
606 carbon emissions from thermokarst lakes and their determinants in the Tibet Plateau, *Global Change*  
607 *Biology*, 2023.

608 Niu, Z., Jinniu, W., Xufeng, W., Dongliang, L., Cheng, S., and Aihong, G.: Net ecosystem CO<sub>2</sub>  
609 exchange and its influencing factors in non-growing season at a sub-alpine forest in the core Three  
610 Parallel Rivers region, *Acta Ecologica Sinica*, 43, 5967-5979, 10.5846/stxb202204020841, 2023.

611 Organization, W. M.: 2019 concludes a decade of exceptional global heat and high-  
612 impactweather[EB/OL].[https://public.wmo.int/en/media/press-release/2019-concludes-decade-of-](https://public.wmo.int/en/media/press-release/2019-concludes-decade-of-exceptional-global-heat-and-high-impact-weather)  
613 [exceptional-global-heat-and-high-impact-weather](https://public.wmo.int/en/media/press-release/2019-concludes-decade-of-exceptional-global-heat-and-high-impact-weather), 2019.

614 Pan, Y., Birdsey, R. A., Fang, J., Houghton, R., Kauppi, P. E., Kurz, W. A., Phillips, O. L., Shvidenko,  
615 A., Lewis, S. L., and Canadell, J. G.: A large and persistent carbon sink in the world's forests,  
616 *Science*, 333, 988-993, 2011.

617 Pavelka, M., Acosta, M., Marek, M. V., Kutsch, W., and Janous, D.: Dependence of the Q10 values  
618 on the depth of the soil temperature measuring point, *Plant and Soil*, 292, 171-179, 10.1007/s11104-  
619 007-9213-9, 2007.

620 Qu, S., Xu, R., Yu, J., and Borjigidai, A.: Extensive atmospheric methane consumption by alpine  
621 forests on Tibetan Plateau, *Agricultural and Forest Meteorology*, 339, 109589,  
622 <https://doi.org/10.1016/j.agrformet.2023.109589>, 2023.

623 Reichstein, M., Falge, E., Baldocchi, D., Papale, D., Aubinet, M., Berbigier, P., Bernhofer, C.,  
624 Buchmann, N., Gilmanov, T., Granier, A., Grünwald, T., Havránková, K., Ilvesniemi, H., Janous,  
625 D., Knohl, A., Laurila, T., Lohila, A., Loustau, D., Matteucci, G., Meyers, T., Miglietta, F., Ourcival,  
626 J.-M., Pumpanen, J., Rambal, S., Rotenberg, E., Sanz, M., Tenhunen, J., Seufert, G., Vaccari, F.,

627 Vesala, T., Yakir, D., and Valentini, R.: On the separation of net ecosystem exchange into  
628 assimilation and ecosystem respiration: review and improved algorithm, *Global Change Biology*,  
629 11, 1424-1439, <https://doi.org/10.1111/j.1365-2486.2005.001002.x>, 2005.

630 Schotanus, P., Nieuwstadt, F. T. M., and De Bruin, H. A. R.: Temperature measurement with a sonic  
631 anemometer and its application to heat and moisture fluxes, *Boundary-Layer Meteorology*, 26, 81-  
632 93, 10.1007/BF00164332, 1983.

633 Schweizer, V. J., Ebi, K. L., van Vuuren, D. P., Jacoby, H. D., Riahi, K., Strefler, J., Takahashi, K.,  
634 van Ruijven, B. J., and Weyant, J. P.: Integrated Climate-Change Assessment Scenarios and Carbon  
635 Dioxide Removal, *One Earth*, 3, 166-172, 10.1016/j.oneear.2020.08.001, 2020.

636 Schwinning, S. and Sala, O. E.: Hierarchy of responses to resource pulses in arid and semi-arid  
637 ecosystems, *Oecologia*, 141, 211-220, 10.1007/s00442-004-1520-8, 2004.

638 Stein, T.: Carbon dioxide peaks near 420 parts per million at Mauna Loa observatory, NOAA  
639 Research, June, 7, 2021.

640 Tang, X., Xiao, J., Ma, M., Yang, H., Li, X., Ding, Z., Yu, P., Zhang, Y., Wu, C., Huang, J., and  
641 Thompson, J. R.: Satellite evidence for China's leading role in restoring vegetation productivity over  
642 global karst ecosystems, *Forest Ecology and Management*, 507, 120000,  
643 <https://doi.org/10.1016/j.foreco.2021.120000>, 2022.

644 Vote, C., Hall, A., and Charlton, P.: Carbon dioxide, water and energy fluxes of irrigated broad-acre  
645 crops in an Australian semi-arid climate zone, *Environmental Earth Sciences*, 73, 449-465, 2015.

646 Wang, C.-Y., Wang, J.-N., Wang, X.-F., Luo, D.-L., Wei, Y.-Q., Cui, X., Wu, N., and Bagaria, P.:  
647 Phenological Changes in Alpine Grasslands and Their Influencing Factors in Seasonally Frozen  
648 Ground Regions Across the Three Parallel Rivers Region, Qinghai-Tibet Plateau, *Frontiers in Earth  
649 Science*, 9, 10.3389/feart.2021.797928, 2022a.

650 Wang, S., Grant, R., Verseghy, D., and Black, T.: Modelling plant carbon and nitrogen dynamics of  
651 a boreal aspen forest in CLASS—the Canadian Land Surface Scheme, *Ecological Modelling*, 142,  
652 135-154, 2001.

653 Wang, Y., Yao, G., Zuo, Y., and Wu, Q.: Implications of global carbon governance for corporate  
654 carbon emissions reduction, *Frontiers in Environmental Science*, 11, 3, 2023a.

655 Wang, Y., Sun, Y., Chen, Y., Wu, C., Huang, C., Li, C., and Tang, X.: Non-linear correlations exist

656 between solar-induced chlorophyll fluorescence and canopy photosynthesis in a subtropical  
657 evergreen forest in Southwest China, *Ecological Indicators*, 157, 111311,  
658 <https://doi.org/10.1016/j.ecolind.2023.111311>, 2023b.

659 Wang, Y., Xiao, J., Ma, Y., Ding, J., Chen, X., Ding, Z., and Luo, Y.: Persistent and enhanced carbon  
660 sequestration capacity of alpine grasslands on Earth's Third Pole, *Science Advances*, 9,  
661 eade6875, doi:10.1126/sciadv.ade6875, 2023c.

662 Wang, Y., Xiao, J., Ma, Y., Luo, Y., Hu, Z., Li, F., Li, Y., Gu, L., Li, Z., and Yuan, L.: Carbon fluxes  
663 and environmental controls across different alpine grassland types on the Tibetan Plateau,  
664 *Agricultural and Forest Meteorology*, 311, 108694, 2021.

665 Wang, Z. Y., Li, Z. Y., Dong, S. K., Fu, M. L., Li, Y. S., Li, S. M., Wu, S. N., Ma, C. H., Ma, T. X.,  
666 and Cao, Y.: Evolution of ecological patterns and its driving factors on Qinghai-Tibet Plateau over  
667 the past 40 years, *Acta Ecologica Sinica*, 42, 8941-8952, 2022b.

668 Wehr, R., Munger, J. W., McManus, J. B., Nelson, D. D., Zahniser, M. S., Davidson, E. A., Wofsy,  
669 S. C., and Saleska, S. R.: Seasonality of temperate forest photosynthesis and daytime respiration,  
670 *Nature*, 534, 680-683, 10.1038/nature17966, 2016.

671 Wu, T., Ma, W., Wu, X., Li, R., Qiao, Y., Li, X., Yue, G., Zhu, X., and Ni, J.: Weakening of carbon  
672 sink on the Qinghai-Tibet Plateau, *Geoderma*, 412, 115707,  
673 <https://doi.org/10.1016/j.geoderma.2022.115707>, 2022.

674 Yasin, A., Niu, B., Chen, Z., Hu, Y., Yang, X., Li, Y., Zhang, G., Li, F., and Hou, W.: Effect of  
675 warming on the carbon flux of the alpine wetland on the Qinghai-Tibet Plateau, *Frontiers in Earth  
676 Science*, 10, 10.3389/feart.2022.935641, 2022.

677 YU, G. and SUN, X.: Principles of flux measurement in terrestrial ecosystem, Beijing: Higher  
678 Education Press, 2006.

679 Yu, Y.: Double-order system construction of China's climate change legislation under the dual  
680 carbon goals, *China Population Resources and Environment*, 32, 89-96, 2022.

681 Zemin, Z., Fenggui, L., Qiong, C., Xingsheng, X., and Qiang, Z.: Spatial Prediction of Potential  
682 Property Loss by Geological Hazards based on Random Forest—A Case Study of Chamdo, Tibet,  
683 *Plateau Science Research*, 7, 21-30, 10.16249/j.cnki.2096-4617.2023.02.003, 2023.

684 Zhang, J., Lin, H., Li, S., Yang, E., Ding, Y., Bai, Y., and Zhou, Y.: Accurate gas extraction (AGE)

685 under the dual-carbon background: Green low-carbon development pathway and prospect, Journal  
686 of Cleaner Production, 134372, 2022.

687 Zhang, Y., Zhu, W., Sun, X., and Hu, Z.: Carbon dioxide flux characteristics in an *Abies fabri* mature  
688 forest on Gongga Mountain, Sichuan, China, *Acta Ecologica Sinica*, 38, 6125-6135, 2018.

689

690